Radiation Measurements 155 (2022) 106784

Contents lists available at ScienceDirect

Radiation Measurements

journal homepage: www.elsevier.com/locate/radmeas

Investigation of quartz luminescence properties in bedrock faults: Fault slip processes reduce trap depths, lifetimes, and sensitivity

Margaret L. Odlum [a,*], Tammy Rittenour [b], Alexis K. Ault [b], Michelle Nelson [b], Evan J. Ramos [c]

[a] Department of Geoscience, University of Nevada, Las Vegas, NV, USA
[b] Department of Geosciences, Utah State University, Utah, USA
[c] Department of Earth, Environmental and Planetary Sciences, Rice University, Texas, USA

A B S T R A C T

Quantitative constraints on the timing and temperatures associated with Quaternary fault slip inform earthquake mechanics and seismic hazard analyses. Optically stimulated luminesce (OSL) and thermoluminescence (TL) are tools that can provide these constraints from fault gouge and localized slip surfaces. This study investigates the quartz luminescence properties of five 2-mm-thick slices of rock as a function of distance perpendicularly from a discrete, m-scale mirrored fault surface that cuts quartz-rich conglomerate along the Hurricane fault, UT, USA. We use pulsed annealing linearly modulated OSL experiments to determine the response of OSL signals to annealing temperatures. Results were used to estimate trap depths and trap lifetimes. We also calculated changes in OSL and TL sensitivity across the fault-perpendicular transect. All five subsamples show a strong initial fast component peak following annealing steps of 200–300 °C, which is absent following higher pre-heat steps of 320–420 °C. The fast component trap lifetimes and depths indicate they are stable over the Quaternary and suitable for OSL dating. Data exhibit increasing trap depth, trap lifetime, and sensitivity with distance from the fault surface. We suggest mechanical processes, fluids, and/or elevated temperatures during seismicity work constructively to transform fault materials and affect the quartz luminescence properties at a mm-scale from this fault surface. Results highlight the importance of assessing the scale of fault-related impacts on host rock and luminescence properties when applying trapped-charge techniques to recover fault-slip chronologies and/or paleotemperature information.

1. Introduction

Documenting the timing of Quaternary fault slip and evidence of coseismic frictional heating is important for understanding active tectonics and earthquake dynamics, and assessing seismic hazards (e.g., Savage et al., 2014; McDermott et al., 2017; Scharer and Yule, 2020; Burgette et al., 2020). Optically stimulated luminescence (OSL) and thermoluminescence (TL) analyses use specific minerals, such as quartz and feldspar, which can trap unbound electrons within crystalline defects when minerals are exposed to ionizing environmental radiation (e.g., Huntley et al., 1985; Rhodes, 2011; Murray et al., 2021). The trapped electrons are evicted when the mineral is exposed to light or heat, or experiences mechanical stress or high pressures (see review by Murray et al., 2021). During seismic slip, trapped electrons in minerals within fault material may be evicted due to friction-generated heat and/or mechanical deformation (e.g., Singhvi et al., 1994; Rink et al., 1999; Spencer et al., 2012; Kim et al., 2019; Yang et al., 2019). Luminescence measured in the lab, by stimulating mineral grains with light (OSL) or heat (TL), is proportional to the time since the last resetting, allowing the OSL and TL signals to provide information on timing and/or temperatures of these events. OSL and TL have an effective dating range of 10^1–10^6 years (e.g., Rittenour, 2008; Rhodes, 2011) and an ultralow temperature sensitivity of ~35–60 °C (Guralnik et al., 2013; King et al., 2016) which makes these techniques especially well-suited for Quaternary fault geochronology and thermometry.

Previous luminescence studies have constrained the timing of past seismic events accommodated in fault gouge (Singhvi et al., 1994; Spencer et al., 2012; Ganzawa et al., 2013; Tsakalos et al., 2020) and shown reduction in OSL and TL signals in experimentally sheared samples (Toyoda et al., 2000; Kim et al., 2019; Yang et al., 2019; Oohashi et al., 2020). Laboratory experiments explored the relationships between slip rates and signal loss, and attribute OSL and TL signal loss to friction-generated heat (Yang et al., 2019; Oohashi et al., 2020). The effects of mechanical stresses and grinding as a resetting mechanism have been explored in fault gouge (Toyoda et al., 2000; Hiraga et al., 2002), but have not been investigated in highly localized slip surfaces that develop in bedrock. In natural fault rocks, faulting processes and fluid-rock interactions can change the physical and chemical properties of the rocks (Caine et al., 1996; Faulkner et al., 2010; Rowe and Griffith, 2015; Ault, 2020). These changes may affect the luminescence properties of quartz including the types of traps, signal profiles (i.e., proportions of fast, medium, or slow-decay components), quartz sensitivity,

* Corresponding author.
E-mail address: margo.odlum@unlv.edu (M.L. Odlum).

https://doi.org/10.1016/j.radmeas.2022.106784
Received 15 December 2021; Received in revised form 21 April 2022; Accepted 2 May 2022
Available online 12 May 2022

and trap depths and lifetimes. Understanding these properties, and how they may be affected by fault-slip related processes such as coseismic temperature rise, fluid-rock interactions, and grain size reduction, is critical for interpreting OSL and TL results from natural fault rocks.

In this study, we investigate and quantify the luminescence properties and luminescence signal components of quartz in fault rocks that are relevant to optical dating and trapped charge thermochronometry using a linear modulated (LM) OSL technique (Jain et al., 2003; Singarayer and Bailey, 2003). We apply a high-spatial resolution (mm-scale) sampling approach to a m-scale fault mirror (polished and straited plane) along the seismogenic Hurricane fault, southwestern UT. Samples from the silicified, quartz-rich conglomerate host rock were not previously exposed to light. We demonstrate that the quartz luminescence-component properties change significantly with perpendicular distance from the fault surface and coincide with physical changes in the quartz grains that developed during past fault-slip events. Constraining the luminescence components in fault rocks is important for understanding OSL and TL signal changes and signal loss, as well as the applicability of OSL and TL methods for deriving fault-slip paleotemperatures and/or dating the timing of fault-slip events.

2. Hurricane fault, samples, and sample preparation

The Hurricane fault is a north–south trending, 250 km-long segmented west-dipping normal fault that extends from southern Utah to northern Arizona (Fig. 1A). Deformation along Hurricane fault initiated during the late Miocene or early Pliocene in association with Basin and Range extension in the western USA (Stewart and Taylor, 1996; Fenton et al., 2001; Lund et al., 2007; Biek et al., 2010). The Hurricane fault is part of the Intermountain Seismic Belt and is seismically active, and there have been at least 20 earthquakes > M4 occurring in southwestern Utah over the past century (Fig. 1A; Christenson and Nava, 1992).

In the study area, the fault juxtaposes the Timpoweap Member, including the Rock Canyon Conglomerate, of the Triassic Moenkopi Formation in the footwall and the Lower Red Member of the Moenkopi Formation in the hanging wall (Fig. 1B; Biek et al., 2010). The studied bedrock fault is located along Utah state highway 9 near La Verkin, UT, (37.22 N, −113.26 W) where the fault is expressed as several *en echelon*, meters-high (~1–6 m), mirrored fault surfaces (Fig. 1). The striated fault-rock surfaces have smooth, highly reflective surfaces known as fault mirrors, with areas of hematite mineralization (Taylor et al., 2021). Prior detailed multiscale textural and (U–Th)/He thermochronometry from patches of hematite precipitated along a mirrored fault plane ~112 m north from our sample provided evidence of up dip propagation of earthquake ruptures through ~300 m depth at ~0.65–0.40 Ma (Taylor et al., 2021).

We targeted a sample within the Rock Canyon Conglomerate that contained two parallel, mirrored fault surfaces (outer and inner mirrors, Fig. 1C–E) that strike SSE and are subvertical. Importantly, a portion of the inner mirror was not exposed to light (i.e., host rock on both sides of the fault are present). The exposed portion of the inner fault surface that was visible was characterized as a striated, highly reflective silica-rich fault mirror (Fig. 1C and D). We assume that the concealed portion of

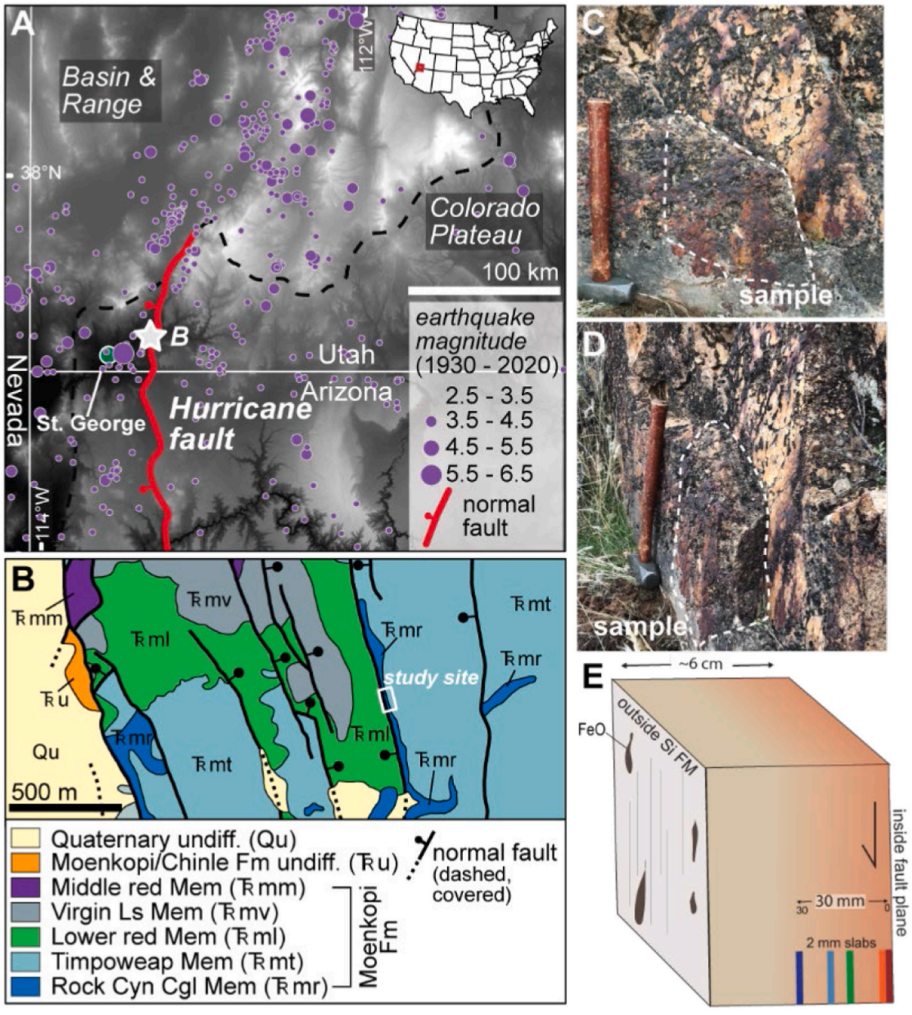

Fig. 1. (a) Digital elevation model with the Hurricane fault and 1930–2020 earthquake catalog; purple circles indicate epicenter and are scaled to earthquake magnitude. White star denotes study area (modified after Koger and Newell, 2020 and Taylor et al., 2021) (b) Simplified geologic map modified from Biek (2003). White box is the study area (Modified from Taylor et al., 2021). (c–d) Field photographs of targeted, mirrored fault surfaces; (e) cartoon diagram showing the sample and the 2 mm thick sample slabs analyzed in this study.

this same fault plane is similar, so our sampled conjugate fault surface likely exhibits the same surface morphology. The fault-rock sample was collected at night under a light-safe tarp and immediately wrapped in aluminum foil, secured with tape, and placed in a light-safe container.

All sample preparation and analysis took place at the Utah State University (USU) Luminescence Laboratory. In a dark lab, the outermost 2.5 cm along the edges of the rock were cut off using a tile saw to remove any potential light exposed portions. A 5.5 x 4-cm-portion of the remaining rock was subsampled in a fault perpendicular transect by cutting 2-mm-thick slabs parallel to the fault surface for 3 cm (for a total of 15 subsamples) using a slow-speed, water-cooled saw in a dark lab. The slabs were soaked in 30% HCl for 12–24 h to remove any carbonate cement and then gently disaggregated with a ceramic mortar and pestle. The 90–250 μm size fraction was separated by wet sieving and then treated with 30% HCl for 1–12 h to remove any remaining $CaCO_3$. Quartz was isolated using sodium polytungstate heavy liquid (2.7 g/cm^3) and subsequently etched in 48% HF followed by 37% HCl to remove any fluorite precipitants. A subset of the final separates was imaged using a field-emission scanning electron microscope equipped with energy x-ray dispersive detector in the USU Microscopy Core Facility to ensure they were pure quartz.

3. Experimental details

We analyzed five subsamples from 0 to 2 mm (USU-3442), 2–4 mm (USU-3443), 12–14 mm (USU-3448), 18–20 mm (USU-3451), and 28–30 mm (USU-3456) away from the fault surface using a pulsed annealing, linear modulated OSL (PA-LM-OSL) experiment (Table 1). Luminescence measurements were made on Risø TL/OSL Model DA-20 readers, with stimulation by blue-green light emitting diodes (LED; 470 ± 30 nm) and luminescence signal detection through 7.5-mm UV filters (U-340).

Three aliquots of sand-sized (90–250 μm) quartz grains covering 5 mm diameter regions (~500 grains/aliquot) on stainless steel discs were analyzed from each of the subsamples. Our analytical routine (Table 1) followed a similar procedure of Bulur et al. (2000) and Singarayer and Bailey (2003) where aliquots were preheated to increasingly higher preheat temperatures to look at the thermal stability of the luminescence signals in each subsample. Following a laboratory dose (~50 or ~25 Gy) aliquots were heated to temperatures that ranged between 200 °C and 420 °C in 20 °C increments (5 °C/s ramp rate, held for 10 s), each followed by a LM-OSL measurement to determine the remnant OSL of the fast-decay signal component (Fig. 2). The LM-OSL analysis was performed for 400 s at 125 °C with blue LEDs light (λ = 470 nm) with stimulation power increased linearly from 0 reaching a maximum of 50 mW/cm^2. To ensure signals were fully bleached between each step, an additional continuous wave OSL of 100 s at 320 °C was carried out between each measurement to bleach the OSL to negligible levels. A subsequent LM-OSL analysis following a dose of 20 Gy and 160 °C preheat was used to monitor sensitivity changes throughout the measurement procedure and compare OSL sensitivity among samples (test dose step). We also measured the TL during the pre-heating steps to investigate TL responses and sensitivities among samples.

The temperature-dependent retention lifetime of a trap type, assuming first order kinetics, is given by Equation (1) (Singarayer, 2002; Singarayer and Bailey, 2003).

$$\tau = s^{-1} \exp\left(\frac{E}{kT}\right) \quad (1)$$

where τ is the lifetime (s), s is the frequency factor (s^{-1}), E is trap depth (eV), T is temperature (K), and k is Boltzmann's constant (~ 8:615 × 10^{-5} eV K^{-1}) (Singarayer, 2002; Singarayer and Bailey, 2003).

Table 1
Pulsed annealing, linear modulated OSL (PA-LM-OSL) experiment details.

STEP	TREATMENT	PURPOSE
1	Initial bleach at 320 °C (470 nm LEDs @ 38 mW/cm^2) for 100s	Bleach natural signal
2	Beta irradiate for 250 s	Give ~25 Gy lab dose
3	Pre-heat sample to 200 °C (+20 °C in each consecutive run) and hold for 10s; measure TL during heating	Annealing step to check for luminescence change in response to temperature treatment
4	Measure LM-OSL (0–50 mW/cm^2) for 400 s at 125 C	Characterize the signal components of the remnant OSL
5	Bleach at 320 °C (470 nm LEDs @ 38 mW/cm^2) for 100s	bleach any remaining signal
6	Beta irradiate for 250 s	give ~25 Gy lab dose for repeated test dose
7	Pre-heat sample to 160 °C for 10s (measure TL during heating)	Pre-heat for test dose
8	Measure LM-OSL (0–50 mW/cm^2) for 400 s at 125 °C	LM-OSL sensitivity monitor of fast component
9	Bleach at 320 °C (470 nm LEDs @ 38 mW/cm^2) for 100s	bleach any remaining signal
10	return to step 2	

The sensitivity-corrected OSL was plotted as a function of preheating temperature to obtain pulse-annealing curves (Fig. 3A). Assuming the total LM-OSL emitted is proportional to the remnant trapped charge, n, the remnant OSL following pre-heating to a temperature T can be described by Equation (2) (derived in Singarayer, 2002):

$$n = n_0 \exp\left[\left(\frac{-skT^2}{\beta E}\exp\left(\frac{-E}{kT}\right)\right) + \left(\frac{skT_0{}^2}{\beta E}\exp\left(\frac{-E}{kT_0}\right)\right)\right] \quad (2)$$

The variable n_0 is the initial trapped charge concentration, T_0 is the ambient room temperature (~20 °C = 288 K) and β is the heating rate. We use this equation to generate curve fits to the pulsed annealing data that inform estimates of the trap parameters E and s, and then calculate trap lifetimes at 20 °C using Equation (1).

4. Results

Data from three aliquots from each subsample were normalized for sensitivity differences and the corresponding LM-OSL signals were averaged to produce a composite LM-OSL curve (Fig. 2). This mean LM-OSL curve for each subsample was used to calculate the thermal stabilities, trap lifetimes, and sensitivities.

4.1. Pulsed annealing (PA) curves

The PA-LM-OSL curves show a large variation in brightness between samples, but the dominant signal-component peaks occur in a similar position and the overall shape of the curves are similar. For example, the curves following pre-heating to 200–300 °C are characterized by an initial strong peak from ~0 to 15 s (fast component), with a maximum intensity around ~8–9 s, followed by second, lower intensity peak typically from 100 to 150 s (Fig. 2). The curves after pre-heating to 320–420 °C show little to no fast-component signal (Fig. 2; S1–S5).

The LM-OSL curves were separated into first order components using *fit_LMCurve*, a routine for the nonlinear least squares fits to LM-OSL curves (Kitis et al., 2008; Kreutzer, 2022) in the R "Luminescence" package (Friedrich et al., 2021). Fitting is given by Equation (3) (Kitis et al., 2008; Kreutzer, 2022):

$$y = \left[\left(\exp(0.5) \times Im_1 \times \frac{x}{xm_1}\right) \times \exp\left(\frac{-x^2}{2*xm_1^2}\right)\right] + , \ldots , + \left[\left(\exp(0.5) \times Im_i \times \frac{x}{xm_i}\right) \times \exp\left(\frac{-x^2}{2*xm_1^2}\right)\right] \quad (3)$$

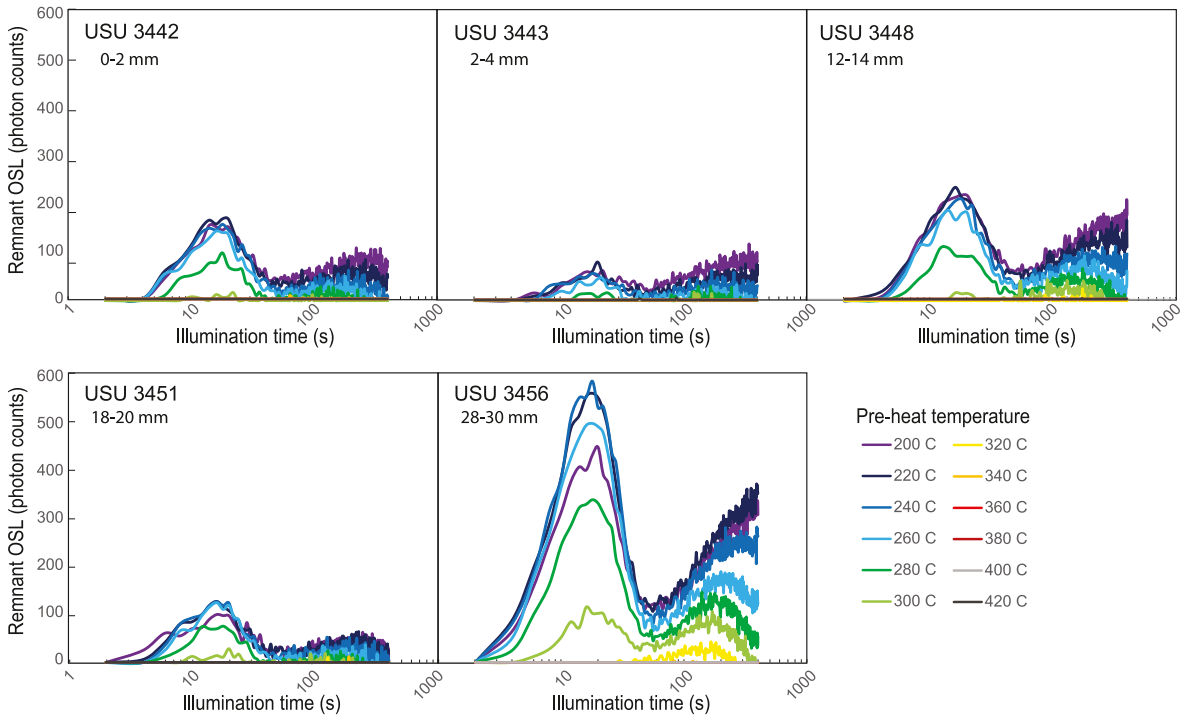

Fig. 2. Pulsed annealing LM OSL at 470 nm from five quartz samples at different distances from the fault place measured at 160 °C, following 25 Gy and preheats between 200 and 420 °C.

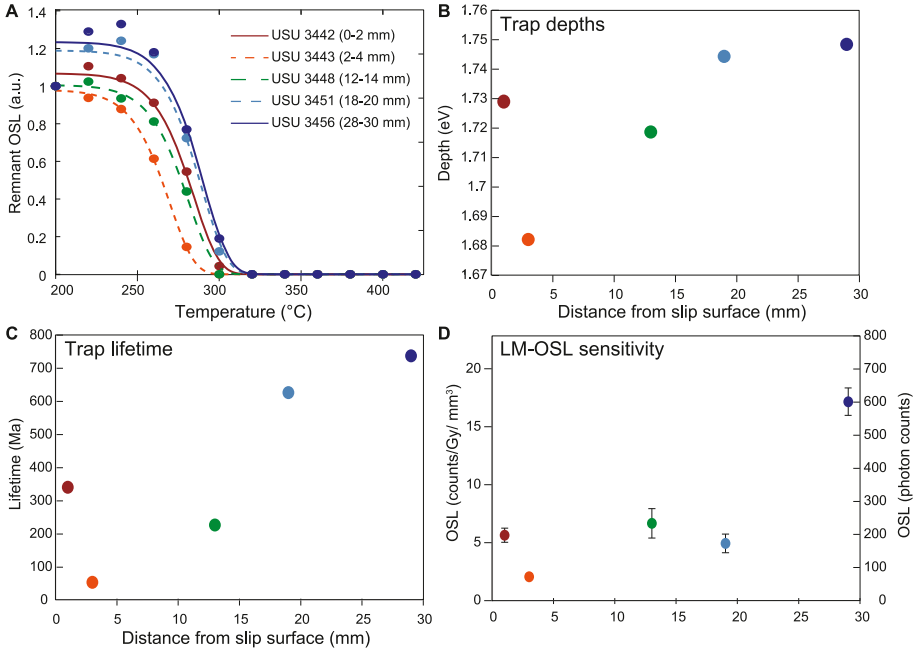

Fig. 3. (a) Calculated pulse annealing curves (remnant LM-OSL versus preheat temperature) for the fast component of each sample. Circle symbols are empirical data (symbols), and lines (solid and dashed) are fits to the data. (b) Estimated trap depths in eV from the model fits in a. (c) Estimated fast component trap lifetimes in Myr calculated using Equation (1) in the text. (d) LM-OSL fast component sensitivity following 25 Gy and a preheats between 160 °C.

where $1 < i < 8$ *and.*

$$xm_i = \sqrt{\frac{\max(t)}{b_i}}$$

$$Im_i = \exp(-0.5)\frac{n_0}{xm_i}$$

We used the default starting parameters for the optical de-trapping probability (b) and dimensionless factor proportional to the initially trapped charge concentration (n) deduced from published values of quartz samples (Jain et al., 2003). The curve separation yields values for the peak position and peak maximum intensity for each component following the formulas in Kitis and Pagonis (2008). For our subsamples, LM-OSL curves following pre-heating to 200–300 °C can be fit with two components (representing a fast and slow decay component; Figs. S1–S5). Samples USU 3442, 3443, 3451, and 3456 can be fit with

three components only after the 200 °C pre-heat step (Fig. S6). The second component from the three-component fit does not overlap with the first component at the fitted peak intensity. The curves following higher pre-heating steps of 320–420 °C do not yield fits for a fast-component owing to little to no remnant fast-component.

Results from annealing steps that produced signal component fits (<300 °C) illustrate that the first peak observed in the LM-OSL curves represents a single component, which we interpret as the easily bleachable 'fast' component. This is supported by continuous wave OSL (CW-OSL) signals from the same samples following a dose of ~50 Gy and pre-heat step of 200 °C (Fig. S7). The first component peak positions are between 8 and 10 s (~2% power or 1 mW/cm^2), and the intensity from the fit_LMCurve function is used as the remnant OSL for the fast component.

The intensity of the fast component was used to calculate the remnant OSL for each pre-heat step and was normalized to the first 200 °C annealing pre-heat step. Pulsed annealing curves, derived from the normalized and sensitivity-corrected fast component of the LM-OSL, were derived as a function of preheating temperature (Fig. 3A). All five subsamples show similar decay shapes, with sharp decays at annealing pre-heat temperatures >280 °C. Subsamples USU 3442, 3443, and 3448 are stable up 240 °C and display depletion beginning at 260 °C. Subsamples USU 3451 and USU 3456 are stable up to 260 °C. The signal is near zero (or background) for all samples with 320 °C and higher pre-heat treatments.

4.2. Thermal stabilities and trap lifetimes

The pulsed annealing curves were fit using Equation (2). We used a nonlinear regression technique in MATLAB to produce the curve fits and solve for trap depth, *E*, and the frequency factor, *s* (Fig. 3A; Table 2). All subsamples yield similar estimates for *s* of ~5.2 x 10^{13} s^{-1}. The estimated values for *E* range between 1.68 and 1.75 eV. Values of *E* are highest in the two samples farthest from the fault slip surface. These estimates are consistent with *E* and *s* values from sedimentary quartz (Singarayer and Bailey, 2003) and from natural amorphous and microcrystalline silicon dioxide (generally termed "silex") (Schmidt and Kreutzer, 2013). The *E* and *s* values were then used to calculate the trap lifetimes using Equation (1). The trap lifetimes range between ~50 and 740 Myr with the trend as a function of distance from the fault plan mirroring trends in trap depths (greatest trap lifetimes farthest from the fault plane).

4.3. OSL and TL sensitivity

Sensitivity changes in individual aliquots during the experiment are minor for pre-heat steps up to 380 °C (<15%), with increased sensitivity (typically <20%) after the 400 and 420 °C pre-heat steps. The OSL sensitivity was calculated from the mean of the fast component peak of the LM-OSL curve following a given dose of 20 Gy and 160 °C preheat. These measurements were performed after each incremental LM-OSL pre-heat annealing step. Fig. 3 shows the average subsample fast component intensities. Subsample average fast-component OSL sensitivities are ~2–20 counts/Gy/mm^3, with highest sensitivity in the sample farthest from the slip surface (Fig. 3D). Fig. 4A illustrates the TL glow curves, following the given radiation dose and measured during the 420 °C pre-heat steps and the signal intensities of the 110 °C and 275 °C peaks are shown in Fig. 4B and C, respectively. There is a clear trend in increasing TL sensitivity with depth away from the slip surface in the glow curves and both the 110 °C and 275 °C peaks.

5. Discussion

5.1. Variations in quartz luminescence parameters

LM-OSL curves from all five samples can be fit with prominent fast and slow decay components. The pulsed annealing LM-OSL curves show that the OSL signal increases slightly during the 220–240 °C pre-heat steps and above 280 °C the signal decreases rapidly until it is close to zero (or background) at 320 °C. This is consistent with most of the fast component OSL signal originating from a trap that corresponds to the rapid bleaching thermoluminescence (TL) peak at about 325 °C (310 °C at 5 °C/s; Smith et al., 1986; Wintle and Murray, 1999). The ability to fit the pulsed annealing curves with Equation (2) supports the prediction that the fast component follows first-order kinetics. Estimates for *E* and *s* from the pulsed annealing LM-OSL data-fits indicate all samples have thermal stabilities and trap lifetimes sufficient to allow dating through the Quaternary.

The LM-OSL curves and the component fits indicate the presence of a harder to bleach, or slower decay, component(s) at annealing temperatures of 200–300 °C (Fig. 2). The calculated trap depths and lifetimes are lower than the fast component. Samples USU 3442, 3443, 3448, and 3451 are not adequately stable for dating sediments on Quaternary timescales (see Supplemental Material Fig. S8 and Table S1) (Singarayer and Bailey, 2003).

We observe variations in the pulsed annealing curves, estimated trap depths, trap lifetimes, and sensitivities between subsamples and, particularly, as a function of distance from the slip surface. We note that the quartz grains are detrital and therefore have natural variability in provenance (i.e., volcanic, plutonic, metamorphic, or recycled sedimentary quartz). We assume that this natural variability is present and evenly distributed within our samples. Thus, variations in the luminescence parameters observed in our experiments are attributed to the post-depositional and post-lithification history the quartz experienced. Importantly, the trap depths and lifetimes vary as a function of depth from the fault surface. For example, both parameters are lowest in the first 14 mm from the fault surface and increase significantly at distances >18 mm (Fig. 3B and C). The calculated trap lifetimes increase by a factor of ~2–3 between 0 and 14 mm and >18 mm (Fig. 3C). Subsamples from 18 to 20 mm (USU 3451) and 28–10 (USU 3456) mm depths yield similar values and are the most thermally stable, which we interpret are representative of the undeformed host rock values. We suggest that the decrease in thermal stability and lifetimes in subsamples USU 3442, USU 3443, and USU 3448 are due to fault slip related processes that affected the rock volume and quartz within ~14 mm of the slip surface.

There are only minor sensitivity changes during the experiments for pre-heat steps up to 380 °C for each aliquot, but there is an increase in

Table 2
Estimates of fast component parameters. Detrapping probability (b) and photoionization cross section (σ) from the *fit_LMcurve* function outputs. *E* and *s*, derived from fitting the pulsed annealing curves in Fig. 3A.

Subsample	Depth from fault	b (s^{-1})	σ (cm^2)	s (s^{-1})	E (eV)	Lifetime at 20 °C (Ma)
USU 3442	0–2 mm	2.67	3.13E-17	5.20E+13	1.73	340
USU 3443	2–4 mm	3.24	3.80E-17	5.20E+13	1.68	53
USU 3448	12–14 mm	2.79	3.28E-17	5.20E+13	1.72	226
USU 3451	18–20 mm	2.98	3.50E-17	5.20E+13	1.74	626
USU 3456	28–30 mm	2.66	3.13E-17	5.20E+13	1.75	737

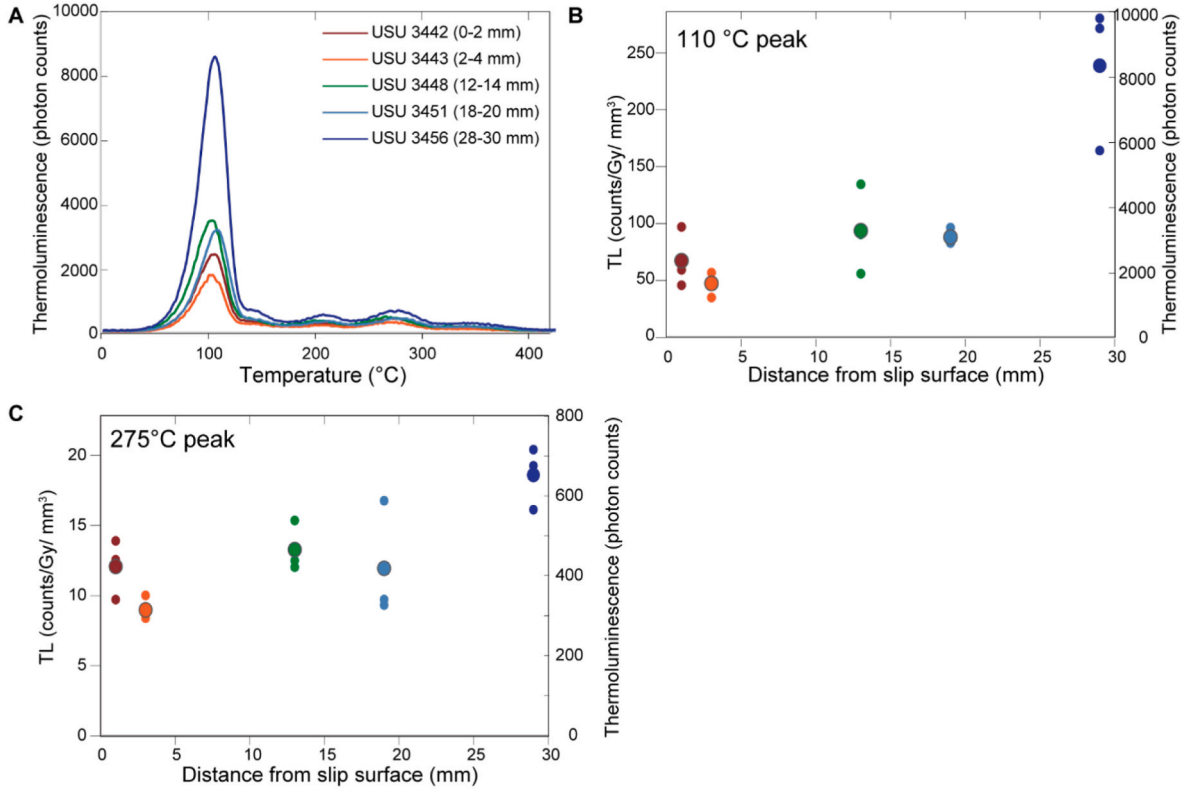

Fig. 4. (a) Thermoluminescence glow curves following 25 Gy, measured during the 420 °C pre-heat step. (b–c) TL sensitivity calculated from the glow curves as a function of depth from the fault plane for the 110 °C peak (b) and 275 °C peak (c). Small symbols are single aliquot measurements and large symbol is the sample mean.

sensitivity (typically <20–100%) after the 400 and 420 °C pre-heat steps. Temperature-induced changes in the OSL sensitivity of natural quartz can occur and have been attributed to thermal annealing (e.g., Botter-Jensen et al., 1995, 1996; Wintle and Murray, 1999). Prior studies indicate that this sensitization is most significant at temperatures of 500–800 °C, with only minor effects observed in the temperature ranges of our annealing pre-heat temperatures (Botter-Jensen et al., 1995). Experiment pre-heat treatments <500 °C and sensitivity increases only observed during the final two pre-heat steps collectively support that the sensitivity variations between samples are natural and not laboratory heating induced.

Similar to the trap depths and lifetimes determined from the pulsed annealing curves, both OSL and TL sensitivities from test doses show a general positive relationship between sensitivity and distance from the fault surface (Figs. 3D and 4). Several pre-dose (that is, not induced in the laboratory) factors can affect quartz sensitivity including the physical, chemical, and thermal environment during crystallization (Sawakuchi et al., 2011), and heating, photobleaching, and/or irradiation in nature (Wintle and Murray, 1999; Bøtter-Jensen et al., 1995; Pietsch et al., 2008; Mineli et al., 2021). These treatments cause charge-transfer between defects and/or the formation of new centers that modulate charge trapping and recombination process (e.g., Sharma et al., 2017) and luminescence pathways can be altered over geologic times (Rink, 1994). Sensitivity can also be affected by chemical impurities in the quartz (e.g., Al, Fe; Takashi et al., 2006) and it is anti-correlative to water content (Sharma et al., 2017). Because the sensitivity is related to the nature and concentration of intrinsic defects like vacancies and interstitials in the crystal lattice of a mineral, we infer that quartz crystallinity can affect sensitivity. Microcrystalline and amorphous silica would have lower sensitivity than macrocrystalline quartz. We hypothesize that observed differences in sensitivity reflect physical differences caused by post-depositional changes in the quartz (silica) as a function of to distance from the fault surface.

5.2. Luminescence characteristics relation to faulting

Our results indicate that OSL and TL sensitivity are lower within 14 mm of the fault surface and increase ≥18 mm away from the fault. This reflects the post-depositional thermal, chemical, and physical history of this quartz, in particular immediately adjacent to the slip surface. The

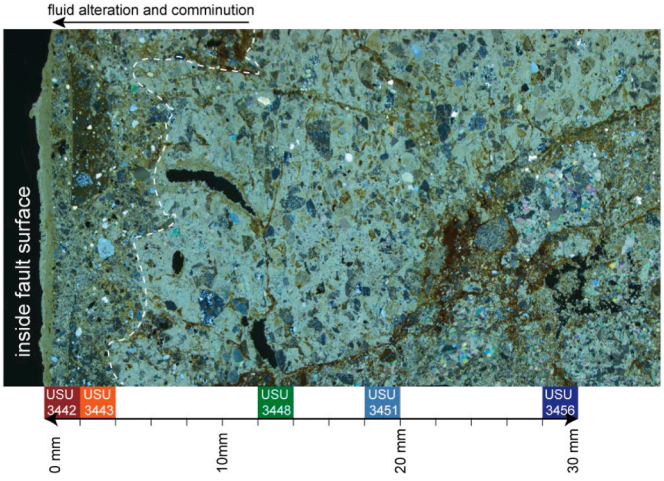

Fig. 5. Thin section photomicrograph in cross-polarized light of the fault rock (taken adjacent to slabs where analyzed quartz came from). The fault plane is at the left side of the image. The yellow and brownish colors are FeO, light to dark grey grains are quartz, lightest grey matrix is mostly calcite, and black are void spaces. There is significant comminution of the quartz particles and evidence of fluid alteration within the first ~3 mm from the fault plane.

three subsamples closest to the fault place show decreased thermal stability and lifetimes of the traps when compared to the farthest subsamples (e.g., USU 3456). We suggest that physical, and possibly chemical, transformations of the quartz assisted by mechanical, thermal, and fluid-related processes operative during slip along the fault surface are responsible for the differences in luminescence properties.

We observe petrologic and textural evidence of physical changes to the host rock and fluid alteration within the first few mm of the fault surface (Fig. 5). In thin section, extreme grain comminution (i.e., grain size reduction) and presence of Fe-oxide near the fault surface reflect mechanical changes to the quartz and alteration, respectively (Fig. 5). We hypothesize that fault slip and fluids present during deformation reduced the grain size and likely impacted the crystallinity of the quartz minerals, affecting the nature and concentration of luminescence traps). Hydrous crystalline silica and amorphous silica have been observed along other silica-rich fault mirrors associated with extreme grain size reduction (i.e., mechanical amorphization; e.g., Kirkpatrick et al., 2013; Houser et al., 2021). The presence of hydrous and/or amorphous silica along our investigated fault surface may manifest in the observed trends in luminescence properties with distance from the fault. Detailed micro-to nanoscale characterization of the quartz grains near and away from the fault surface is required to confirm this hypothesis.

Our results highlight that, in localized bedrock faults, mechanical processes including amorphization, fluids, and/or elevated temperatures that likely accompany seismicity (Taylor et al., 2021) transform fault materials and affect the quartz luminescence properties over mm-length scales. Laboratory deformation experiments demonstrate that shearing at seismic slip rates can induce partial to complete OSL and TL signal loss, attributed to frictional temperature rise (Yang et al., 2019; Oohashi et al., 2021). Our data indicate that in natural fault rocks, mechanical processes (e.g., comminution, mechanical amorphization) and fluid alteration (e.g., precipitation of FeO, silicification) also affect the luminesce properties. Investigating these properties is critical not only for characterizing and comparing natural OSL and TL signals and equivalent doses, but also for informing the physical and geochemical transformations that occur during faulting.

6. Conclusions

Pulsed annealing linearly modulated OSL and TL measurements of quartz from high spatial resolution samples as a function of distance from a brittle fault surface were used to estimate the trap depth, frequency factor, trap lifetimes, and sensitivities of quartz luminescence signals on a localized fault mirror along the Hurricane fault that cuts a quartz-rich conglomerate. Trap depth, lifetime, and OSL and TL sensitivity are generally lowest within 14 mm of the fault surface and increase at distances $\geq$18 mm from the fault interface. We interpret these patterns to reflect the post-depositional history of the fault rock, most likely arising from physical changes in the quartz that resulted from faulting. These processes include comminution, mechanical amorphization, fluid-rock interaction, and frictional heating that likely worked constructively to change originally detrital quartz grains within ~14 mm of the fault surface. Data suggest rock texture and mineral structure changes affect the quartz luminescence properties. Our work illustrates it is important to quantify these properties to understand OSL and TL signals and to ultimately use quartz luminescence techniques to calculate ages and/or temperatures from fault rocks.

Declaration of competing interest

The authors declare that they have no known competing financial interests or personal relationships that could have appeared to influence the work reported in this paper.

Acknowledgements

This work was supported by a National Science Foundation Postdoctoral Fellowship awarded to MLO (award #1952905). We are grateful for reviews from Reza Sohbati and Sumiko Tsukamoto for thoughtful reviews that led to an improved manuscript. We thank Tomas Capaldi, Dennis Newell, and Madison Taylor for their help in the field and insightful discussions, Christoph Schmidt and Georgina King for insightful discsussions, and Maggie Erlick and Michael Strange for assistance in the lab.

Appendix A. Supplementary data

Supplementary data to this article can be found online at https://doi.org/10.1016/j.radmeas.2022.106784.

References

Ault, A.K., 2020. Hematite fault rock thermochronometry and textures inform fault zone processes. J. Struct. Geol. 133, 104002.
Biek, R., Rowley, P., Hayden, J., Hacker, D., Willis, G., Hintze, L., et al., 2010. Geologic Map of the St. George and East Part of the Clover Mountains, 30' X 60' Quadrangles, Washington and Iron Counties, Utah. Utah Geological Survey, Salt Lake City, UT.
Bøtter-Jensen, L., McKeever, S.W.S., 1996. Optically stimulated luminescence dosimetry using natural and synthetic materials. Radiat. Protect. Dosim. 65 (1–4), 273–280.
Bøtter-Jensen, L., Larsen, N.A., Mejdahl, V., Poolton, N.R.J., Morris, M.F., McKeever, S. W.S., 1995. Luminescence sensitivity changes in quartz as a result of annealing. Radiat. Meas. 24 (4), 535–541.
Bulur, E., Bøtter-Jensen, L., Murray, A.S., 2000. Optically stimulated luminescence from quartz measured using the linear modulation technique. Radiat. Meas. 32, 407–411.
Caine, J.S., Evans, J.P., Forster, C.B., 1996. Fault zone architecture and permeability structure. Geology 24 (11), 1025–1028.
Christenson, G.E., Nava, S.J., 1992. Earthquake Hazards of Southwestern Utah.
Faulkner, D.R., Jackson, C.A.L., Lunn, R.J., Schlische, R.W., Shipton, Z.K., Wibberley, C. A.J., Withjack, M.O., 2010. A review of recent developments concerning the structure, mechanics and fluid flow properties of fault zones. J. Struct. Geol. 32 (11), 1557–1575.
Fenton, C.R., Webb, R.H., Pearthree, P.A., Cerling, T.E., Poreda, R.J., 2001. Displacement rates on the toroweap and Hurricane faults: implications for quaternary downcutting in the grand Canyon, Arizona. Geology 29 (11), 1035–1038.
Friedrich, J., Mercier, N., Philippe, A., Riedesel, S., Autzen, M., Mittelstrass, D., Gray, H. J., Galharret, J., 2021. Luminescence: comprehensive luminescence dating data analysis. R package version 0.9.16. https://CRAN.R-project.org/package=Luminescence.
Ganzawa, Y., Takahashi, C., Miura, K., Shimizu, S., 2013. Dating of active fault gouge using optical stimulated luminescence and thermoluminescence. J. Geol. Soc. Jpn. 119, 714–726.
Guralnik, B., Jain, M., Herman, F., Paris, R.B., Harrison, T.M., Murray, A.S., Valla, P.G., Rhodes, E.J., 2013. Effective closure temperature in leaky and/or saturating thermochronometers. Earth Planet Sci. Lett. 384, 209–218.
Hiraga, S., Morimoto, A., Shimamoto, T., 2002. Stress effect on thermoluminescence intensities of quartz grains—for the establishment of a fault dating method. Bull. Nara Univ. Educ. Nat. Sci. 51 (2), 17–24.
Houser, L.M., Ault, A.K., Newell, D.L., Evans, J.P., Shen, F.A., Van Devener, B.R., 2021. Nanoscale textural and chemical evolution of silica fault mirrors in the wasatch fault damage zone, Utah, USA. G-cubed 22 (3) e2020GC009368.
Huntley, D.J., Godfrey-Smith, D.I., Thewalt, M.L., 1985. Optical dating of sediments. Nature 313 (5998), 105–107.
Jain, M., Murray, A.S., Bøtter-Jensen, L., 2003. Characterization of blue-light stimulated luminescence components in different quartz samples: implications for dose measurement. Radiat. Meas. 37 (4–5), 441–449.
Kim, J.H., Ree, J.H., Choi, J.H., Chauhan, N., Hirose, T., Kitamura, M., 2019. Experimental investigations on dating the last earthquake event using OSL signals of quartz from fault gouges. Tectonophysics 769, 228191.
Kirkpatrick, J.D., Rowe, C.D., White, J.C., Brodsky, E.E., 2013. Silica gel formation during fault slip: evidence from the rock record. Geology 41 (9), 1015–1018.
Kitis, G., Pagonis, V., 2008. Computerized curve deconvolution analysis for LM-OSL. Radiat. Meas. 43 (2–6), 737–741.
Kreutzer, S., 2021. In: Kreutzer, S., Burow, C., Dietze, M., Fuchs, M.C., Schmidt, C., Fischer, M. (Eds.), fit_LMCurve( ): Nonlinear Least Squares Fit for LM-OSL Curves. Function Version 0.3.3.
Lund, W.R., Hozik, M.J., Hatfield, S.C., 2007. Paleoseismic Investigation and Long-Term Slip History of the Hurricane Fault in Southwestern Utah, vol. 119. Utah Geological Survey.
McDermott, R.G., Ault, A.K., Evans, J.P., Reiners, P.W., 2017. Thermochronometric and textural evidence for seismicity via asperity flash heating on exhumed hematite fault mirrors, Wasatch fault zone, UT, USA. Earth Planet Sci. Lett. 471, 85–93.
Murray, A., Arnold, L.J., Buylaert, J.-P., Guérin, G., Qin, J., Singhvi, A.K., Smedley, R., Thomsen, K.J., 2021. Optically stimulated luminescence dating using quartz. Nat. Rev. 1 (72), 1–31.

Oohashi, K., Minomo, Y., Akasegawa, K., Hasebe, N., Miura, K., 2020. Optically stimulated luminescence signal resetting of quartz gouge during subseismic to seismic frictional sliding: a case study using granite-derived quartz. J. Geophys. Res. Solid Earth 125 (10) e2020JB019900.
Pietsch, T.J., Olley, J.M., Nanson, G.C., 2008. Fluvial transport as a natural luminescence sensitiser of quartz. Quat. Geochronol. 3 (4), 365–376.
Rhodes, E.J., 2011. Optically stimulated luminescence dating of sediments over the past 200,000 years. Annu. Rev. Earth Planet Sci. 39, 461–488.
Rink, W.J., 1994. Billion-year age dependence of luminescence in granitic quartz. Radiat. Meas. 23 (2–3), 419–422.
Rink, W.J., Toyoda, S., Rees-Jones, J., Schwarcz, H.P., 1999. Thermal activation of OSL as a geothermometer for quartz grain heating during fault movements. Radiat. Meas. 30 (1), 97–105.
Rittenour, T.M., 2008. Luminescence dating of fluvial deposits: applications to geomorphic, palaeoseismic and archaeological research. Boreas 37 (4), 613–635.
Rowe, C.D., Griffith, W.A., 2015. Do faults preserve a record of seismic slip: a second opinion. J. Struct. Geol. 78, 1–26.
Savage, H.M., Polissar, P.J., Sheppard, R., Rowe, C.D., Brodsky, E.E., 2014. Biomarkers heat up during earthquakes: new evidence of seismic slip in the rock record. Geology 42 (2), 99–102.
Sawakuchi, A.O., Blair, M.W., Dewitt, R., Faleiros, F.M., Hyppolito, T., Guedes, C.C.F., 2011. Thermal history versus sedimentary history: OSL sensitivity of quartz grains extracted from rocks and sediments. Quat. Geochronol. 6 (2), 261–272.
Schmidt, C., Kreutzer, S., 2013. Optically stimulated luminescence of amorphous/microcrystalline SiO2 (silex): basic investigations and potential in archeological dosimetry. Quat. Geochronol. 15, 1–10.
Sharma, S.K., Chawla, S., Sastry, M.D., Gaonkar, M., Mane, S., Balaram, V., Singhvi, A.K., 2017. Understanding the reasons for variations in luminescence sensitivity of natural quartz using spectroscopic and chemical studies. Proc. Indian Natl. Sci. Acad. 83, 645–653.
Singarayer, J.S., Bailey, R.M., 2003. Further investigations of the quartz optically stimulated luminescence components using linear modulation. Radiat. Meas. 37 (4–5), 451–458.
Singarayer, J.S., 2002. Linearly Modulated Optically Stimulated Luminescence of Sedimentary Quartz: Physical Mechanisms and Implications for Dating. D.Phil. Thesis. University of Oxford, unpublished.
Singhvi, A.K., Banerjee, D., Pande, K., Gogte, V., Valdiya, K.S., 1994. Luminescence studies on neotectonic events in south-central Kumaun Himalaya—a feasibility study. Quat. Sci. Rev. 13 (5–7), 595–600.
Smith, B.W., Aitken, M.J., Rhodes, E.J., Robinson, P.D., Geldard, D.M., 1986. Optical dating, methodological aspects. Radiat. Protect. Dosim. 17, 229–233.
Spencer, Joel QG., Hadizadeh, Jafar, Gratier, Jean-Pierre, Doan, Mai-Linh, 2012. Dating deep? Luminescence studies of fault gouge from the San Andreas Fault zone 2.6 km beneath Earth's surface. Quat. Geochronol. 10, 280–284.
Stewart, M.E., Taylor, W.J., 1996. Structural analysis and fault segment boundary identification along the Hurricane fault in southwestern Utah. J. Struct. Geol. 18 (8), 1017–1029.
Taylor, M.P., Ault, A.K., Odlum, M.L., Newell, D.L., 2021. Shallow rupture propagation of pleistocene earthquakes along the Hurricane fault, UT, revealed by hematite (U-Th)/He thermochronometry and textures. Geophys. Res. Lett. 48 (17) e2021GL094379.
Toyoda, S., Rink, W.J., Schwarcz, H.P., Rees-Jones, J., 2000. Crushing effects on TL and OSL on quartz: relevance to fault dating. Radiat. Meas. 32 (5–6), 667–672.
Tsakalos, E., Lin, A., Kazantzaki, M., Bassiakos, Y., Nishiwaki, T., Filippaki, E., 2020. Absolute dating of past seismic events using the OSL technique on fault gouge material—a case study of the nojima fault zone, SW Japan. J. Geophys. Res. Solid Earth 125 (8) e2019JB019257.
Wintle, A.G., Murray, A.S., 1999. Luminescence sensitivity changes in quartz. Radiat. Meas. 30 (1), 107–118.
Yang, H.L., Chen, J., Yao, L., Liu, C.R., Shimamoto, T., Jobe, J.A.T., 2019. Resetting of OSL/TL/ESR signals by frictional heating in experimentally sheared quartz gouge at seismic slip rates. Quat. Geochronol. 49, 52–56.

Further reading

Burgette, R.J., Hanson, A.M., Scharer, K.M., Rittenour, T.M., McPhillips, D., 2020. Late Quaternary slip rate of the Central Sierra Madre fault, southern California: Implications for slip partitioning and earthquake hazard. Earth Planet Sci. Lett. 530, 115907.
King, G.E., Guralnik, B., Valla, P.G., Herman, F., 2016. Trapped-charge thermochronometry and thermometry: A status review. Chem. Geol. 446, 3–17.
Koger, J.M., Newell, D.L., 2020. Spatiotemporal history of fault–fluid interaction in the Hurricane fault, western USA. Solid Earth 11 (6), 1969–1985.
Mineli, T.D., Sawakuchi, A.O., Guralnik, B., Lambert, R., Jain, M., Pupim, F.N., Del Rio, I., Guedes, C.C.F., Nogueira, L., 2021. Variation of luminescence sensitivity, characteristic dose and trap parameters of quartz from rocks and sediments. Radiat. Meas. 144, 106583.
Scharer, K.M., Yule, D., 2020. A maximum rupture model for the southern San Andreas and San Jacinto faults, California, derived from paleoseismic earthquake ages: Observations and limitations. Geophys. Res. Lett. 47 (15) e2020GL088532.
Biek, R., 2003. Geologic Map of the Hurricane Quadrangle Washington County. *Utah: Utah Geological Survey Map, 187.*